

1 Advancements in Hydrogel Applications for Mechanobiological Research and Mechanomedicine

2
3 Oleg Kolosov 1*

4 1 Nanoscience, Physics Department, Lancaster University, United Kingdom.

5
6 E-mail: o.kolosov@lancaster.ac.uk

7
8
9
10 **Abstract**

11 Background: Photopolymerised poly(2-Methacryloyloxyethyl phosphorylcholine) (MPC) hydrogels have gained significant
12 interest in biomedical applications, particularly in mechanobiology and mechanomedicine, due to their tunable mechanical
13 properties and biocompatibility. This study aims to investigate the swelling and mechanical behaviors of poly(MPC)
14 hydrogels crosslinked with different agents to assess their suitability for biomedical applications. Methods: Two sets of
15 photopolymerised MPC hydrogels were synthesized by free-radical polymerization under ultraviolet (UV) light (365 nm,
16 3200 W/m²) for 10 minutes using 0.5 w/v% 2,2-Dimethoxy-2-phenylacetophenone (DMPA) as a photoinitiator. In the first
17 experiment, 25 w/v% MPC was crosslinked with pentaerythritol tetraacrylate (PETA) at varying concentrations. In the
18 second experiment, the same MPC concentration was crosslinked with tetraethylene glycol dimethacrylate (TEGDMA).
19 Hydrogel appearance and chemical composition were characterized using attenuated total reflectance Fourier-transform
20 infrared (ATR-FTIR) spectroscopy. Swelling volume and rheological properties were assessed after two days of swelling in
21 distilled water at room temperature. In a third experiment, 3 v/v% propargyl methacrylate (PgMA) was polymerized with
22 25 w/v% MPC and 15 v/v% TEGDMA, and alkyne group incorporation was confirmed via ATR-FTIR. Results: Poly(MPC-
23 PETA) appeared white, whereas poly(MPC-TEGDMA) was transparent. ATR-FTIR spectra confirmed successful
24 polymerization by identifying the functional groups in MPC, PETA, and TEGDMA. Both poly(MPC-PETA) and poly(MPC-
25 TEGDMA) hydrogels exhibited a decrease in swelling volume and an increase in storage modulus with higher crosslinker
26 concentrations. The poly(PgMA-MPC-TEGDMA) hydrogel exhibited a storage modulus of 31.6 Pa, and the presence of
27 alkyne groups was confirmed by ATR-FTIR analysis. Conclusion: This study demonstrates that poly(MPC) hydrogels exhibit
28 tunable swelling and mechanical properties depending on the type and concentration of crosslinkers used. The findings
29 provide valuable insights for optimizing hydrogel formulations for biomedical applications, particularly in mechanobiology
30 and mechanomedicine.

31 Keywords: Photopolymerisation, MPC hydrogels, Swelling behavior, Mechanical properties, Biomedical applications

32
33
34 **Significance**

35 This study provides insights into optimizing photopolymerised MPC hydrogels for biomedical applications in
36 mechanobiology and mechanomedicine, enhancing material design.

37
38
39
40
41
42

43
44
45
46
47
48
49
50
51
52
53
54
55
56
57
58
59
60
61
62
63
64
65
66
67
68
69
70
71
72
73
74
75
76
77
78
79
80
81
82
83
84

Introduction

Hydrogels, a polymeric material that formed by the cross-link network of hydrophilic polymer chains, are either transparent or colloidal gels that can swell large amounts of water. Hydrogels are important biomaterials that has been employed in a number of biomedical applications, due to the excellent biocompatibility, the high permeability for water, and the physical characteristic similarity to soft tissue. Typical applications include cell encapsulation, tissue regeneration scaffolds and biosensors. (Nguyen K.T. and West J.L., 2002)

Cell encapsulation in biodegradable hydrogels provides many useful properties for tissue engineering, such as the tissue-like environment for cells and tissues growth, the ability to form in vivo and the convenience of handling. For example, photopolymerising hydrogel system of poly(ethylene oxide)-dimethacrylate and poly(ethylene glycol) semi-interpenetrating network has shown to be an efficient way to encapsulate bovine and ovine chondrocytes. After one day of encapsulation, chondrocyte survival and a dispersed cell population composed of ovoid and elongated cells were observed; after two weeks, a functional extracellular matrix was present. These results demonstrate the practicability of photoencapsulation for tissue engineering (Elisseff J. and McIntosh W. et al., 2000).

Tissue regeneration scaffold. Hydrogels scaffold has been designed to achieve tissue-like elastic environments that are similar to cartilage and bone, providing the biological environment and influencing different types of cell interactions in tissue engineering. Elisseff J. and Anseth K. et al. (1999) have shown that over two weeks of culture cells distributed evenly throughout the hydrogel scaffolds and extracellular matrix production increased. Moreover, the streaming potentials, dynamic stiffness and equilibrium moduli of tissues increased as culture time increased, which demonstrates the promising hydrogels scaffolds for cartilage regeneration and replacement. Hydrogel tissue scaffolds can also be produced from self-assembled biopolymer networks, which has close similarities with the extracellular matrix in terms of chemical, structural and mechanical properties (Silva R., Fabry B. and Boccaccini A.R., 2014). Additionally, the fibrous protein-based hydrogels have shown excellent biocompatibility, degradability in human body by proteolytic enzymes. These attractive features suggest that the fibrous protein hydrogels can be one of the most versatile biomaterials for tissue engineering.

Rapid and sensitive detection of chemical and biological analysts plays an important role in medical diagnostics. Three dimensional hydrogel binding matrices, providing a larger binding capacity and lower steric hindrance, show a faster sensor response to the affinity binding of target molecules than the two-dimensional surface architecture (Wang Y. and Huang C. et al., 2010). A novel biosensor based on hydrogel optical waveguide spectroscopy (HOWS) was investigated. By using a

85 surface plasmon response (SPR) optical setup, the biosensor was implemented in a carboxylated poly(N-
86 isopropylacrylamide) (PNIPAM) hydrogel film that was attached on a metallic surface and modified by protein catcher
87 molecules through amine coupling chemistry. The swollen micrometre hydrogels acted as a binding matrix and optical
88 waveguide. HOWS has shown a significant improvement in refractive index measurement resolution and binding capacity,
89 due to the low damping and high swelling ratio. Recently, a self-assembling three-dimensional peptide hydrogel was
90 developed as a 3D solid support where oligonucleotides can be immobilised and be used to detected complementary
91 sequences, allowing 22pM of detection limit. Moreover, the biomolecule detection under biological environment was
92 achieved as the unique properties of peptide hydrogels minimised unwanted probe-probe interaction. Further investigation
93 in this technique can potentially contribute to detection of other smaller biomolecules in area such as biomedical diagnostics,
94 drug identification and pollutants in environmental monitoring.

95 Hydrogels are formed by crosslinking between polymer chains. It can be classified based on the type of cross-link junctions:
96 physical crosslinking or chemical crosslinking. Physically cross-link junctions are reversible bonding that formed by
97 entanglements and attractions between polymer chains, whereas chemical junctions are chemical bonding that formed
98 permanently between one or more monomers. Crosslinkers containing acrylate groups, such as pentaerythritol tetraacrylate
99 and tetraethylene glycol dimethacrylate, are commonly seen in hydrogel synthesis, as they are crosslinkable moieties and
100 relatively sensitive to free radical polymerisation (Bartolo P. and Bidanda B., 2008).

101 Methacryloyloxyethyl phosphorylcholine (MPC) is one of the most suitable monomers which has been widely employed in
102 biomedical applications. MPC contains a phosphorylcholine group in the side chain allowing it to mimic the phospholipid
103 polar groups in cell membranes, hence MPC block copolymers are biocompatible in nature and shows desirable interaction
104 with living tissues (Sigma-Aldrich, 2016). Recently, a functional poly(MPC) hydrogel, copolymerised with propargyl
105 methacrylate (PgMA), was developed as a potential candidate in biosensing applications. It has been proven that specific
106 target molecules, streptavidin and DNA, were detected using a surface plasmon resonance technique (Wiarachai O et al.,
107 2015).

108 Photopolymerisation process is a common technique that employed in hydrogel formation, where monomers are converted
109 into polymers under the exposure of ultraviolet (UV) light. The major advantage of photopolymerisation is that hydrogels
110 can be produced in situ from aqueous with a minimal degree of invasion (Nguyen K.T. and West J.L.). For instance, by using
111 catheter (Hill-West J.L. et al., 1994; West J.L. and Hubbell J.A., 1996) and laparoscopic device (Hill-West J.L. et al., 1994),
112 complex shapes can be formed and adhered on tissue structures, which is particularly attractive for numerous biomedical
113 applications. In addition, temporal and spatial control over polymerisation is enable, allowing fast curing at room
114 temperature or physiological temperature and low heat production (Decker C., 2001).

115 Photoinitiation are classified based on photolysis mechanisms, including photocleavage, hydrogen abstraction, and cationic
116 polymerisation (Fouassier J.P., 1995). Photopolymerisation process requires the usage of photoinitiators, light-sensitive
117 compounds that can create free radicals under UV exposure. Considerations in selecting photoinitiators include high
118 absorption efficiency at specific wavelength, solubility in water, biocompatibility, stability and cytotoxicity (Scranton A.B. et
119 al., 1996). Photoinitiators are added to initiate the polymerisation reaction, followed by the propagation of polymer chain
120 and growth of longer chains. Moreover, photoinitiators also show low cytotoxicity, which allows the polymerisation of a cell
121 suspension and hence the encapsulation of viable cells within hydrogels (Pathak C.P. et al., 1992). Examples of cells that have
122 been successfully encapsulated in hydrogels are fibroblasts (Lutolf M.P. et al., 2003; Lutolf M.P. and Hubbell J.A., 2005),
123 smooth muscle cells (Mann B.K. et al., 2001; Mann B.K. and West J.L., 2003; Peyton S.R. et al., 2006), osteochondrocytes and
124 their progenitors (Elisseff J. et al., 2005; Yang F. et al., 2005; Sharma B. et al., 2007).

125 Properties of hydrogels that are particularly considered for biomedical applications include biocompatibility, equilibrium
126 swelling ratio, and mechanical properties.

127 Biocompatibility and nontoxicity are crucially vital for the application of hydrogels in biomedical field. Biocompatibility
128 consists bio-safety and bio-functionality, which is the ability of a material to perform the specific task for the application
129 with an appropriate host response that is not only systemic but also local (Nilimanka D., 2013). If the biocompatible property
130 of hydrogels is not achieved in tissue engineering, where tissue is constructed via cellular regeneration and scaffold
131 degradation, the hydrogel maybe fouled and the connected tissue maybe damaged.

132 A challenge of in vivo biocompatibility is the incomplete conversion of toxic chemicals added during the fabrication of
133 hydrogels, where host cells may be subject to toxicity concerns if initiators, organic solvents, unreacted monomers and cross-
134 linkers leach out to tissue and encapsulated cells during applications (Nilimanka D.). It has been reported that Irgacure 2959,
135 a photoinitiator, reduce the viability of cells when the applied concentration exceeds 0.1% (Yin H. et al., 2010). To optimise
136 the detrimental effects of hazardous chemical compounds, resulting hydrogels must be purified by extensive solvent washing
137 or dialysis. Alternatively, the concerns of photoinitiator may be eliminated by forming hydrogels via radiation (Nilimanka
138 D.). Cytotoxicity and in vivo toxicity tests must be passed for hydrogels to be practically applicable. Cytotoxicity test, known
139 as the in vitro cell culture tests, is used to examined the compatibility of implanted biomaterials. In vivo toxicity test is
140 assessed by the knowledge of chemical composition in hydrogel and conditions of tissue exposure (Nilimanka D.).

141 Chemical structure of hydrogels can be identified by Attenuated Total Reflectance – Fourier Transformed Infrared
142 Spectroscopy (ATR-FTIR) can be used to identified. The principle is that the chemical bonds of a substance can be excited
143 and absorb infrared light at specific frequencies that can characterise the types of chemical bonds. Therefore, the resulting
144 IR spectrum is the fingerprint of measured sample. This technique is useful for the identification of chemical structure of
145 hydrogels and the comparison with the starting chemical substances (Torres R. et al., 2003; Mansur H.S. et al., 2004).

146 Swelling is defined as the amount of water taken-up by the hydrogels, which influence the dimension of hydrogels directly
147 and further affect the mechanical properties. For example, lower volume-swelling ratios is often observed stiffer hydrogels.
148 Swelling behaviour of hydrogels demonstrates the hydrophobicity of the polymer network and the relative density of the
149 crosslinking network (Carlibria S.R. and Burdick J.A., 2016). Physical texture of hydrogels is altered by the environmental
150 conditions such as pH, temperature, electric signal and presence of enzyme or ionic species. Changes in volume is driven by
151 the changes in solvent pH and the concentration difference between mobile ions in hydrogel interior and external solution.
152 Fluctuations in external environmental pH can affect the behaviour of acidic or basic functional groups in hydrogels, leading
153 to changes in degree of ionisation of functional groups and hence variations in hydrogel volume (Nilimanka D.).

154 Hydrogel swelling ratio can be studied either by the changes in volume or mass of gels. Determination of volume-swelling
155 ratio is straightforward: three dimensions of hydrogels are measured at a time and the volumes are measured, followed by
156 repeating measurements for several times at a fix period of time and until the volume of hydrogels reach at a plateau (typically
157 at room temperature equilibrium swelling is observed within 48 hours). Mass-swelling ratio is obtained by weighting the wet
158 weight (M_w) of blotted hydrogel, and the dry weight (M_d) of the dried hydrogel. The mass-swelling ratio (M_w/M_d) is defined
159 as the ratio of the wet weight to the dry weight of hydrogel; the volumetric swelling ratio (QV) is calculated by the equation:
160 $QV=1+\frac{\rho_{pp}}{\rho_s}(M_w/M_d-1)$, where ρ_{pp} and ρ_s are the densities of hydrogel polymer and solvent (Carlibria, S.R. and Burdick,
161 J.A.).

162 Mechanical properties of hydrogels are critical for various biomedical applications, including tendon repairs, wound
163 dressing and drug delivery. Especially for applications in cell culture and cellular mechanotransduction, which converse the
164 mechanical information of microenvironment to biochemical signals that influence the cellular behaviours such as spreading,
165 migration and stem cell differentiation. The desirable hydrogels should have strong mechanical properties that can maintain
166 the physical texture during the delivery of therapeutic moieties for the predetermined period of time, which is achievable by
167 varying the degree of crosslinking (Nilimanka, D.). Higher degree of crosslinking in hydrogel results in stronger hydrogels
168 with more brittle structure. The optimum hydrogels should be relatively strong and yet enough elastic.

169 Hydrogel mechanical properties are often described by the complex dynamics viscosity (η^*). Complex dynamics viscosity
 170 associated with a small amplitude oscillatory shear flow with angular frequency (ω) is defined as $\eta^*=G''-iG'\omega$,
 171 where G'' and G' are the dynamic viscosity and the dynamic rigidity (Walters K.,1975). G'' and G' are also seen as the amount
 172 of energy dissipated and stored in the deformation process, or the relative viscous and elastic components in material
 173 behaviour under given operating conditions (Walters K.).

174 Mechanical behaviour of hydrogels is characterised by rheometers, which is based on the theory of oscillatory shear between
 175 parallel plates developed by Walters. Walters suggests that advantages of parallel plates geometry from an experimental point
 176 of view is that one can change the gap between plates easily; and a series of experiments can be conducted on the same
 177 sample with the same instrument members. Furthermore, from a theoretical point of view, this geometry can accommodate
 178 the inertial effects without difficulties, compared to other geometries. By referring to a set of cylindrical polar co-ordinates
 179 (r,θ,z), two circular plates of radius a are assumed to oscillate at the same angular frequency but with different amplitudes
 180 (Fig.1).

181 The amplitude ratio (ϑ) is defined as $\vartheta=\theta_1/\theta_2$,

182 where θ_1 and θ_2 are the angular amplitude of the upper plate and the lower plate. The phase lag of the upper plate behind
 183 the lower is denoted by c . The test sample is contained between two plates, where the lower one performs small amplitude
 184 forced oscillations and the upper one is constrained. Therefore, the velocity distribution is $v(r)=0$, $v(\theta)=rf(z)ei\omega$, $v(z)=0$,
 185 where the real component is implied. This velocity distribution satisfies the equation of continuity
 186 $1/r\partial\partial r(rv(r))+1/r\partial v\theta\partial\theta+\partial\partial z v(z)=0$.

187 The boundary conditions are $f(0)=i\omega\theta_2eic$, $f(h)=i\omega\theta_1$.

188 At the absence of fluid inertia, f must be satisfied by the differential equation $d^2f/dz^2=0$.

189 Hence the solution is $f=i\omega h[\theta_1-\theta_2eic]z+i\omega\theta_2eic$.

190 The only non-vanishing stress component ($p(\theta z)$) is given by $p(\theta z)=\eta^*r\partial f\partial z e i\omega t$.

191 Solving both equations show that the couple (C) on the top plate is $C=-\eta^*\pi i\omega 2ha^4[\theta_1-\theta_2eic]e i\omega t$.

192 The motion of upper plate is defined as $C=[K-I\omega^2]\theta_1 E i\omega t$,

193 where K is the restoring constant of the torsion wire and I is the moment of inertia of the upper plate about the axis. By
 194 rearranging both equations, one can show that $eic\vartheta=1-i\eta^*S$ where $S=2h[K-I\omega^2]\pi a^4\omega$.

195 Therefore, knowing the amplitude ratio (ϑ) and the phase lag (c) from experiments allows ones to obtain the complex
 196 viscosity (η^*). The formulae of the viscous modulus (G'') and the elastic modulus (G') are the imaginary and the real
 197 component (Walters): $G''=-S\vartheta\text{sinc}[\vartheta^2-2\vartheta\text{cosec}+1]$, $G'=\omega S\vartheta[\text{cosec}-\vartheta][\vartheta^2-2\vartheta\text{cosec}+1]$.

198 Rheological measurements show that, for completely crosslinked hydrogel, 2 regimes of frequency can be observed; the slope
 199 of the curve changes significantly at the transition frequency. The storage modulus of complete obtained always is larger
 200 than the release modulus

201 in the whole range of frequency; whereas incompletely crosslinked hydrogels show higher release modulus than storage
 202 modulus at lower frequencies and lower release modulus at higher frequencies. The difference between the storage modulus
 203 and release modulus at the rubber plateau indicated elastic modulus of three-dimensional crosslinked hydrogel.

204

205 Methods and Materials

206 2-Methacryloyloxyethyl phosphorylcholine (MPC, MW 295.27g/mol) (contains ≤ 100 ppm MEHQ as inhibitor, 97%),
 207 pentaerythritol tetraacrylate (PETA, MW 352.34g/mol) (contains 350 ppm monomethyl ether hydroquinone as inhibitor),
 208 tetraethylene glycol dimethacrylate (TEGDMA, MW 330.37g/mol) ($\geq 90\%$ (GC)), and 2,2-Dimethoxy-2-
 209 phenylacetophenone (DMPA, MW 256.30g/mol) (99%) were purchased from Aldrich Chemistry (USA). Propargyl

210 methacrylate (PgMA, MW 124.14g.mol) (98%, stab. with 250ppm 4-methoxyphenol) was purchased from Alfa Aesor (USA).
211 All chemicals and regents are used as received.

212 *Preparations*

213 For the first stage, two types of poly(MPC) hydrogels were synthesised with different crosslinkers: PETA and TEGDMA. All
214 regents were dissolved in 70% ethanol. Metal spatula was used to take MPC powder; 2.5g of MPC white power was measured
215 by electronic balance and dissolved in 5ml of 70% ethanol, with a concentration of 50 w/v%. Similarly, 1ml of PETA white
216 paste and 1ml of TEGDMA colourless liquid were both measured and dissolved in 2ml of 70% ethanol, with a concentration
217 of 50 v/v%. 0.1g of DMPA white crystal was measured and dissolved in 2ml of 70% ethanol, with a concentration of 5 w/v%.
218 For the second stage of experiments, PgMA-MPC hydrogels was formed with one crosslinker TEGDMA, where all reagents
219 are dissolved in absolute ethanol. 0.5g of MPC was dissolved in 1ml absolute ethanol; 0.5ml of TEGDMA was dissolved in
220 1ml of absolute ethanol; 0.05g of DMPA was dissolved in 1ml of absolute ethanol; and 0.5ml of PgMA was dissolved in 1ml
221 of absolute ethanol, with a concentration of 50 v/v%.

222 All solutions were vortexed for 2 minutes by IKA Vortex Genius 3 until the chemicals were fully dissolved where no large
223 particles were observed in solutions. Finally, the tubes containing solutions were covered with Al foil to avoid light pollution
224 and were prepared for the fabrication of hydrogels.

225 *Fabrications*

226 3 samples were prepared for 1 combination of monomer, crosslinker and photoinitiator in order to avoid possible errors
227 and produce reliable experimental data. Photopolymerisation method was utilised for the fabrication of MPC hydrogels and
228 PgMA-MPC hydrogels. Starting with preparation of the mixture of monomers, crosslinkers and photoinitiators. To
229 investigate the influence of crosslinkers' concentration on swelling and mechanical behaviours, the only variable of
230 experiments was the concentration of crosslinker, which was set to be 3, 6, 9,12, 15 and 18 v/v%. While the concentrations
231 of monomer MPC and photoinitiator DMPA were maintained at 25 w/v% and 0.5 w/v%. For the purpose of mechanical
232 characterisation conducted by rheometers, the diameter of cylindrical hydrogel samples should be the same as the 8mm
233 parallel plate used in the rheometer. A ceramic mould with 8mm diameter and 4mm height was made to contain the solution
234 of polymer mixture for free radical polymerisation; the final volume of hydrogel should be $V=\pi r^2 h=\pi \times 4^2 \times 4=150.72\text{mm}^3$.
235 Aiming to prepare 250 μl of mixture, the volume of each polymer reagent was calculated according the designed
236 concentration, followed by the addition of 70% ethanol solution.

237 Each solution was measured by a micropipette (maximum 200 μl) and added to the precursor solution, mixing by IKA vortex
238 genius 3 (Germany) for approximately 1 minute. Photopolymerisation was initiated by 365nm and 3200 Watt/m²
239 (Spectrolinker XL-1000 UV crosslinker) at room temperature for 10 minutes, which illuminated the precursor solution on
240 ceramic moulds. The photopolymerised hydrogel was removed by metal spatula and rinsed repeatedly with distilled water
241 to remove unreacted solutions, follow by immersing in distilled water at room temperature for swelling studies. For the
242 second stage of experiments, the hydrogel exhibited the strongest mechanical properties was selected to polymerised with
243 PgMA at a final concentration of 3 v/v%. After free radical polymerisation for 10 minute, hydrogel formed was rinsed and
244 immersed with distilled water. To remove residual reagents thoroughly, sample was immersed in distilled and placed on a
245 flat orbital shaker, IKA KS 260 basic (Germany), shook at the speed of 200 rmp for 24 hours at room temperature.

246 *Characterisations*

247 ATR-FTIR. ATR-FTIR spectra of hydrogels were used to confirm the expected functionalities. Spectra were collected with
248 the Thermo Scitific Nicolet iS10 (USA) against a blank KBr pellet background. Samples were removed from distilled water
249 and dried on tissue. Samples were placed on the single reflection diamond ATR accessory (Standard Golden Gate, Specac)
250 as shown in Fig.2; the bridge of equipment was clamped down using the bridge lock screw, ensuring the anvil is clear of the
251 specimen. The anvil was screwed down via the anvil screw, till the screw rotated freely the corrected load was achieved. The

252 software OMNIC was setup to record the sample spectra. ATR-FTIR analysis was performed with 32 scans at a resolution of
 253 4 cm⁻¹ over a frequency range of 400–4000 cm⁻¹. The data spacing was 0.482 cm⁻¹. The characteristic peaks of spectrum
 254 were compared with the literature data to identify the chemical structure of hydrogels.

255 Samples were immersed in distilled water at room temperature for 48 hours to achieve equilibrium swelling. Hydrogels
 256 cylinder were placed in a 6-well plate with one sample per well, with enough room to hydrate freely. Every 24 hour samples
 257 were removed from distilled water and gently blotted to excess liquid. Samples were measured with a digital calliper,
 258 including diameter and height; and placed in fresh distilled water. Measurement of each sample was repeated in 3 times and
 259 average value of dimensions were obtained in order to minimise the error in reading. This process was repeated for 48 hours.
 260 The average volume of hydrogels (V) was calculated using equation: $V = \pi \times (D/2)^2 \times H$,

261 where D and H are average diameter and height of sample. The combined standard error of average volume (ΔV) was
 262 obtained by equation: $\Delta V = V \times \sqrt{[(\Delta H/H)^2 + 12 \times (\Delta D/D)^2]}$,

263 where ΔH and ΔD are standard errors of H and D . Equilibrium swelling (Sv) was calculated with equation: $Sv = V_{\infty} - V_0 V_0$,
 264 where V_{∞} and V_0 are average sample volumes at equilibrium swelling and before swelling. The combined standard error of
 265 equilibrium swelling was obtained using equation: $\Delta Sv = Sv \times \sqrt{[(\Delta V_{\infty})^2 + (\Delta V_0)^2] (V_{\infty} - V_0)^2 + (\Delta V_0 V_0)^2}$,
 266 where ΔV_{∞} and ΔV_0 are standard errors of V_{∞} and V_0 .

267 Hydrogel response to small-amplitude oscillation shear was investigated by TA instruments DISCOVERY HR-1 hybrid
 268 rheometer in 8mm stainless-steel parallel plate geometry (Fig. 3). Samples formed as cylinders were placed between plates.
 269 For frequency sweeping test, storage moduli and loss moduli were monitored as a function of frequency scanning from 0.1
 270 to 100 Hz with 10 points per decade, with oscillation strain of 0.142857% under constant temperature of 25°C. Each hydrogel
 271 sample was tested for two time to reduce the possible errors occurred during rheological measurements.

272 The combined standard error of rheology (ΔG^*) was calculated with equation: $\Delta G^* = 13 \times \sqrt{(\Delta Ga^*)^2 + (\Delta Gb^*)^2 + (\Delta Gc^*)^2}$,
 273 where ΔGa^* , ΔGb^* and ΔGc^* are standard errors of Ga^* , Gb^* , and Gc^* .

274

275 Results and discussions

276 25 w/v% MPC with 3 v/v% PETA solution and 25 w/v% MPC with 3 v/v% TEGDMA solution remained in liquid solution
 277 after UV curing for 10 minutes. Poly(MPC) with 15 v/v%, 18 v/v% PETA and poly(MPC) with 18 v/v% TEGDMA were
 278 fractured during removal from the ceramic mould.

279 ATR-FTIR confirmed characteristic functional groups of MPC, PETA, TEGDMA and PgMA in hydrogels. The chemical
 280 structure of MPC-PETA, MPC-TEGDMA and PgMA-MPC-TEGDMA hydrogels were confirmed by ATR-FTIR
 281 spectroscopy, as presented in Fig.4, 5 and 6. The ATR-FTIR spectra of MPC-PETA hydrogels showed a board band at
 282 3400cm⁻¹ which was assigned to the stretching vibration of the –OH groups from water. The water units also attributed to
 283 two characteristic absorption peaks at 1600cm⁻¹ and 600cm⁻¹. The absorption peaks at 2970cm⁻¹ overlapping with the
 284 board band was attributed to the stretching vibration of –CH₂ or –CH₃ groups. The characteristic peak at 1726cm⁻¹ was
 285 assigned to the stretching vibration of –C=O groups from the acrylate groups appeared in MPC and PETA. The absorption
 286 peaks at 1478cm⁻¹ was due to the bending vibration of –CH₂ or –CH₃ groups. The appearance of absorption peaks at
 287 1230cm⁻¹ and 1070cm⁻¹ were corresponded to the stretching vibration of –O=P-O-asym and –O=P-O-sym of the MPC
 288 units; furthermore, the characteristic peaks at 968cm⁻¹ was attributed to the –N+(CH₃)₃ stretching vibration in the MPC
 289 units. The absorption peak at 1170cm⁻¹ was assigned to the –C-O-C- stretching vibration in the PETA units (Wiarachai O.
 290 et al., 2016). For MPC-TEGDA hydrogels, the absorption peaks observed on the ATR-FTIR spectra were similar to that of
 291 MPC-PETA, due to the high similarity of functional groups in two hydrogels.

292 For PgMA-MPC-TEGDMA hydrogels, the corresponding signals of the PgMA units in ATR-FTIR spectra showed the
 293 absorption peak of the stretching vibration of –C≡C-H groups at 3311cm⁻¹. It was noticed that the peak at 2129cm⁻¹

294 attributed by $-C\equiv C-$ groups of the PgMA units was hardly observed, due to the overlapping with the characteristic peaks of
295 the diamond in the region of 1500cm^{-1} to 2650cm^{-1} . The diamond was used as the reflectance crystal in ATR-FTIR
296 measurements. Moreover, although it was not clearly shown in the spectra, the characteristic absorption peak of $-C=O$
297 groups stretching vibration at 1726cm^{-1} was overlapped with the characteristic peak of the water units at 1636cm^{-1} . The
298 characteristic peaks of the asymmetric $-O=P-O-$ stretching at 1230cm^{-1} and the symmetric $-O=P-O-$ stretching at 1086cm^{-1}
299 for the MPC units were observed. Additionally, the absorption peak at 968cm^{-1} was attributed to the $N+(CH_3)_3$ stretching
300 vibration for the MPC units. These characteristic absorption peaks confirmed the formation of copolymer PgMA-MPC-
301 TEGDMA (Wiarachai O. et al.).

302 Swelling volume of hydrogels reduced with increasing concentration of cross-linkers from 3 v/v% to 15 v/v%. For poly(MPC-
303 PETA) hydrogel and poly(MPC-TEGDMA) hydrogel, significant amount of water content was absorbed on the first day of
304 immersion, whereas only little amount of water was absorbed on the second day. Larger equilibrium swelling volume was
305 obtained in hydrogel with lower concentration of cross-linkers, due to the less hydrophobic crosslinking points (Fig.7 and
306 Fig. 8).

307 Equilibrium swelling of poly(MPC) hydrogel crosslinked with PETA was less than that of poly(MPC) hydrogel crosslinked
308 with TEGDMA using the same concentration of crosslinker (Fig. 9). The molar mass of PETA and TEGDMA are relatively
309 similar, which are 352.34 g/mol and 330.37 g/mol respectively, indicating similar molar concentration of PETA and
310 TEGDMA in the same volume of solution. In one mole of chemicals, PETA has 3 moles of hydrophobic acrylate groups
311 whereas TEGDMA contains 2 moles (Fig.10 and Fig.11). Therefore, comparing between the same concentration of PETA
312 and TEGDMA, poly(MPC-PETA) hydrogel has one mole of hydrophobic crosslinking points more than poly(MPC-
313 TEGDMA) hydrogel, which could weaken the ability of water uptake in the gel network.

314 Swelling kinetic of poly(PgMA-MPC-TEGDMA) was compared with poly(MPC-TEGDMA) (Fig.12). Higher swelling degree
315 was observed with 3 v/v% PgMA; however, theoretically the swellability of poly(PgMA-MPC) should be suppressed by the
316 inherent hydrophobicity of the alkyne moieties in PgMA units (Wiarachai O).

317 Rheological properties, storage moduli and loss moduli, of hydrogels improved with increasing concentrations of
318 crosslinkers 3 v/v% to 15 v/v%. Frequency dependence of elastic storage moduli (G') and viscous loss moduli (G'') for MPC
319 hydrogels at constant temperature of 25°C under an oscillation strain of 0.142857% was depicted in Fig.13. Due to the
320 unstable results of G' and G'' at lower frequency, the sweeping had to be performed in the range of 0.1-100 Hz.

321 Two frequency regimes in the evolution of G' were shown (Fig. 16). In the lower frequency range, G' was nearly frequency
322 independent, suggesting a classic elastic behavior of the hydrogel. Both G' and G'' were relatively low with G' higher than
323 G'' , indicating the elastic component dominated over the viscous component in the region of lower frequency. G' in the
324 region of higher frequency was assumed to be in a linear relationship with higher sweeping frequency. The storage moduli
325 at 0.1Hz (plateau G') increased with increasing concentrations of PETA.

326 Similar to the rheology of MPC-PETA hydrogels, transition of the gradient of G' was observed (Fig.17). In the lower
327 frequency range, G' was approximately frequency independent, whereas G' in the region of higher frequency was linearly
328 proportional to frequency. Both G' and G'' were relatively low at the low frequency range with G'' lower than G' , indicating
329 the three dimensional network formation of elastic hydrogels from crosslinking structure. The plateau G' also increased with
330 concentrations of TEGDMA. However, it was noticed that G'' of 15 v/v% TEGDMA was even higher than the G' of 6 v/v%
331 TEGDMA in the region of 0.1-2Hz; and G' of 15 w/v% TEGDMA was the lowest among 4 concentrations of TEGDMA in
332 the region of 2Hz to 100Hz.

333 Fig.16 and Fig.17 showed the frequency dependence of G' and G'' for poly(MPC-PETA) and poly(MPC-TEGDMA) at
334 various concentration of crosslinkers. When the crosslinking interaction between MPC and crosslinker is completed, both
335 G' and G'' level off, known as a rubber plateau. The constant G' in the lower frequency region suggest entanglement structure

336 was sufficiently formed, producing complete crosslinked and well-developed network in hydrogel (Kim J. and Song J. et al.,
337 2003). At higher frequency, the gradients of all curves with different concentration were parallel, suggesting irrelevant
338 relation between hydrogel network structure and oscillation shear stress at higher frequency. Kim et al. suggested that linear
339 relationship between G' and higher oscillation frequency may due to the partial breakage of the interconnected network,
340 destroyed by the more frequent changes of displacement.

341 **Trending**

342 Poly(MPC) crosslinked with PETA showed lower values of G' than with TEGDMA, while G'' of two hydrogels were relatively
343 similar (Tab.2 and Tab.3). Both poly(MPC) hydrogels exhibited higher G' than G'' over the entire range of concentrations
344 investigated; G' and G'' increased with increasing concentrations of crosslinkers, as well as transition frequency.

345 The plateau G' of hydrogel read at 0.1Hz was increased with the concentration of PETA and TEGDMA (Fig. 18), which
346 echoed the density of chemical crosslinking network in the hydrogel systems. The mechanical properties of 3D network
347 structures formed was the results of the types of interaction including covalent bonding, crystallisation and molecular
348 secondary forces such as hydrogen bonding, molecular entanglements, and hydrophobic interaction (Weng L. et al., 2008).

349 The relative amount of acrylate groups in MPC and crosslinker determined the chemical crosslinking efficiency of gelation
350 and the elastic modulus. The molar mass of MPC molecule and TEGDMA molecule are 295.27 g/mol and 330.37 g/mol
351 respectively. For the 25 w/v% poly(MPC) hydrogel crosslinked with 15 v/v% TEGDMA (T5), the molar concentration (M)
352 are: $MMPC=25295.27=0.0847 \text{ mol/ml}$, $MTEGDMA=15330.37=0.0454 \text{ mol/ml}$.

353 With 1 acrylate group in MPC molecule (seen in Fig.19) and 2 acrylate groups in TEGDMA molecule, the ratio of acrylate
354 groups in MPC ($MA-M$) and TEGDMA ($MA-T$) is $MA-MMA-T=0.0847 \times 10.0454 \times 2=0.0933$,

355 which is approximately 1:1, demonstrating the highest crosslinking efficiency and the highest storage moduli among all the
356 ratios studied. However, it should be mentioned that T5 fractured slightly during handling and poly(MPC) crosslinked with
357 18v/v% was entirely fractured. Although the hydrogel formed with higher concentration of crosslinker exhibited higher
358 storage moduli, meanwhile its fracture stress was lower than other ratios investigated.

359

360 **Conclusion**

361 25 w/v% Poly(MPC) hydrogels crosslinked with PETA and TEGDMA with various concentration were synthesised via
362 photopolymerisation method with DMPA. Hydrogel chemical structures were confirm using ATR-FTIR technique. Results
363 showed that with higher concentration of crosslinker, equilibrium swelling volume was larger and more rigid 3-dimensional
364 structure was formed, due to the higher crosslinking density in hydrogel network. The poly(MPC) hydrogel crosslinked with
365 15 v/v% TEGDMA exhibited the highest elastic modulus and the lowest fracture toughness, indicating the maximum
366 crosslinking efficiency of hydrogel system,. Copolymer poly(PgMA-MPC) was photopolymerised with 15 v/v% TEGDMA,
367 where formation of PgMA units and MPC units in the hydrogel system were confirmed by the FTIR spectra. This results
368 that photopolymerisation process could be a potential synthesis method for poly(PgMA-MPC) hydrogel, which is more
369 beneficial for biomedical applications than other polymerisation methods. Future improvements of photopolymerised
370 poly(PgMA-MPC) hydrogel may focus on quantity analysis of PgMA units in hydrogels, and performances in related
371 applications.

372

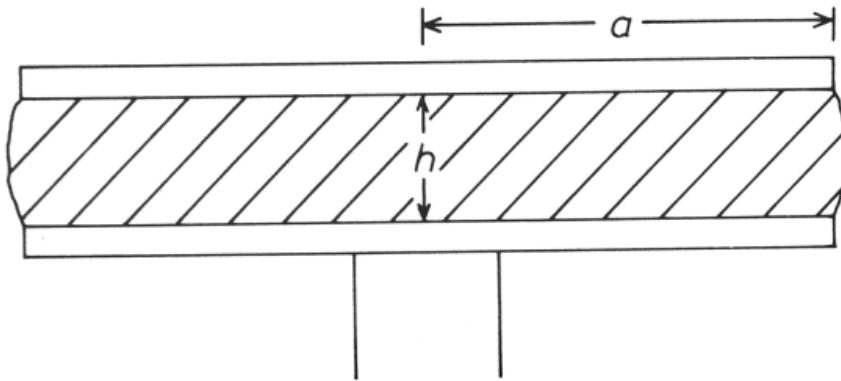
373

374 **References**

- 375 Bartolo, P., & Bidanda, B. (2008). Biomaterials and prototyping applications in medicine. Springer.
376 Caliarì, S. R., & Burdick, J. A. (2016). A practical guide to hydrogels for cell culture. Nature Methods, 13(5), 405.
377 Decker, C. (2001). UV-radiation curing chemistry. Pigment and Resin Technology, 30(5), 278–286.

- 378 Elisseeff, J., & Anseth, K. et al. (1999). Transdermal photopolymerization of poly(ethylene oxide)-based injectable hydrogels
379 for tissue-engineered cartilage. *Plastic and Reconstructive Surgery*, 104, 1014–1022.
- 380 Elisseeff, J., McIntosh, W., Anseth, K., Riley, S., Ragan, P., & Langer, R. (2000). Photoencapsulation of chondrocytes in
381 poly(ethylene oxide)-based semi-interpenetrating networks. *Journal of Biomedical Materials Research*, 51(2), 164–171.
- 382 Elisseeff, J., Puleo, C., Yang, F., & Sharma, B. (2005). Advances in skeletal tissue engineering with hydrogels. *Orthodontics
383 & Craniofacial Research*, 8(3), 150–161.
- 384 Fouassier, J. P. (1995). *Photoinitiation, photopolymerization, and photocuring*. Hanser Publishers.
- 385 Hill-West, J. L., Chowdhury, S. M., Dunn, R. C., & Hubbell, J. A. (1994). Efficacy of a resorbable hydrogel barrier, oxidized
386 regenerated cellulose, and hyaluronic acid in the prevention of ovarian adhesions in a rabbit model. *Fertility and Sterility*,
387 62(3), 630–634.
- 388 Hill-West, J. L., Chowdhury, S. M., Sawhney, A. S., Pathak, C. P., Dunn, R. C., & Hubbell, J. A. (1994). Prevention of
389 postoperative adhesions in the rat by in situ photopolymerization of bioresorbable hydrogel barriers. *Obstetrics &
390 Gynecology*, 83(1), 59–64.
- 391 Hill-West, J. L., Chowdhury, S. M., Slepian, M. J., & Hubbell, J. A. (1994). Inhibition of thrombosis and intimal thickening
392 by in situ photopolymerization of thin hydrogel barriers. *Proceedings of the National Academy of Sciences of the United
393 States of America*, 91(13), 5967–5971.
- 394 Kim, J., Song, J., Lee, E., & Park, S. (2003). Rheological properties and microstructures of Carbopol gel network system.
395 *Colloid and Polymer Science*, 281(7), 614–623.
- 396 King, P. S. J., Saiani, A., Bichenkova, E. V., & Miller, A. F. (2016). A de novo self-assembling peptide hydrogel biosensor with
397 covalently immobilized DNA-recognizing motifs. *Chemical Communications*, 52, 6697.
- 398 Lutolf, M. P., & Hubbell, J. A. (2003). Synthesis and physicochemical characterization of end-linked poly(ethylene glycol)-
399 co-peptide hydrogels formed by Michael-type addition. *Biomacromolecules*, 4(3), 713–722.
- 400 Lutolf, M. P., Schmoekel, J. L., Metters, H. G., Hubbell, A. T., Lauer-Fields, F. E., Fields, G. B., Schmoekel, J. A., & Weber, J.
401 A. (2003). Synthetic matrix metalloproteinase-sensitive hydrogels for the conduction of tissue regeneration: Engineering
402 cell-invasion characteristics. *Proceedings of the National Academy of Sciences of the United States of America*, 100(9), 5413–
403 5418.
- 404 Mann, B. K., & West, J. L. (2002). Cell adhesion peptides alter smooth muscle cell adhesion, proliferation, migration, and
405 matrix protein synthesis on modified surfaces and in polymer scaffolds. *Journal of Biomedical Materials Research*, 60(1),
406 86–93.
- 407 Mann, B. K., Gobin, A. S., Tsai, A. T., Schmedlen, R. H., & West, J. L. (2001). Smooth muscle cell growth in photopolymerized
408 hydrogels with cell adhesive and proteolytically degradable domains: Synthetic ECM analogs for tissue engineering.
409 *Biomaterials*, 22(22), 3045–3051.
- 410 Mansur, H. S., Orefice, R. L., & Mansur, A. A. P. (2004). Characterization of poly(vinyl alcohol)/poly(ethylene glycol)
411 hydrogels and PVA-derived hybrids by small-angle X-ray scattering and FTIR spectroscopy. *Polymer*, 45, 7193–7202.
- 412 Nguyen, K. T., & West, J. L. (2002). Photopolymerizable hydrogels for tissue engineering applications. *Biomaterials*, 23,
413 4307–4314.
- 414 Nilimanka, D. (2013). Preparation methods and properties of hydrogels: A review. *International Journal of Pharmacy and
415 Pharmaceutical Sciences*, 5(3).
- 416 Pathak, C. P., Sawhney, A. S., & Hubbell, J. A. (1992). Rapid photopolymerization of immunoprotective gels in contact with
417 cells and tissue. *Journal of the American Chemical Society*, 114(21), 8311–8312.
- 418 Peyton, S. R., Raub, C. B., Keschrumus, V. P., & Putnam, A. J. (2006). The use of poly(ethylene glycol) hydrogels to
419 investigate the impact of ECM chemistry and mechanics on smooth muscle cells. *Biomaterials*, 27(28), 4881–4893.

- 420 Scranton, A. B., & Bowman, C. N. et al. (1996). Photopolymerization fundamentals and applications. ACS Publishers.
- 421 Sharma, B., Williams, C. G., Khan, M., Manson, P., & Elisseeff, J. H. (2007). In vivo chondrogenesis of mesenchymal stem
422 cells in a photopolymerized hydrogel. *Plastic and Reconstructive Surgery*, 119(1), 112–120.
- 423 Sigma-Aldrich. (2016, September 8). Product descriptions. Retrieved from
424 <http://www.sigmaaldrich.com/catalog/product/aldrich/730114?lang=en®ion=GB>
- 425 Silva, R., Fabry, B., & Boccaccini, A. R. (2014). Fibrous protein-based hydrogels for cell encapsulation. *Biomaterials*, 35(25),
426 6727–6738.
- 427 Torres, R., Usall, J., Teixido, N., Abadias, M., & Viñas, I. (2003). Liquid formulation of the biocontrol agent *Candida sake* by
428 modifying water activity or adding protectants. *Journal of Applied Microbiology*, 94, 330–339.
- 429 Walters, K. (1975). Rheometry. Chapman and Hall.
- 430 Wang, Y., Huang, C., Jonas, U., Wei, T., Dostalek, J., & Knoll, K. (2010). Biosensor based on hydrogel optical waveguide
431 spectroscopy. *Biosensors and Bioelectronics*, 25(7), 1663–1668.
- 432 Weng, L., Chen, L., & Chen, W. (2007, April). Rheological characterization of in situ crosslinkable hydrogels formulated
433 from oxidized dextran and N-carboxyethyl chitosan. *Biomacromolecules*, 8(4), 1109–1115.
- 434 West, J. L., & Hubbell, J. A. (1996, November 12). Separation of the arterial wall from blood contact using hydrogel barriers
435 reduces intimal thickening after balloon injury in the rat: The roles of medial and luminal factors in arterial healing.
436 *Proceedings of the National Academy of Sciences of the United States of America*, 93(23), 13188–13193.
- 437 Wiarachai, O., Vilaivan, T., Iwasaki, Y., & Hoven, V. P. (2016). Clickable and antifouling platform of poly[(propargyl
438 methacrylate)-ran-(2-methacryloyloxyethyl phosphorylcholine)] for biosensing applications. *Langmuir*, 32(4), 1184–1194.
- 439 Yang, F., Williams, C. G., Wang, D., Lee, H., Manson, P. N., & Elisseeff, J. (2005). The effect of incorporating RGD adhesive
440 peptide in polyethylene glycol diacrylate hydrogel on osteogenesis of bone marrow stromal cells. *Biomaterials*, 26(30), 5991–
441 5998.
- 442 Yin, H., Gong, C., Shi, S., Liu, X., Wei, Y., & Qian, Z. (2010). Toxicity evaluation of biodegradable and thermosensitive PEG-
443 PCL-PEG hydrogel as a potential in situ sustained ophthalmic drug delivery system. *Journal of Biomedical Materials
444 Research Part B*, 92, 129–137.
- 445
- 446
- 447
- 448
- 449
- 450
- 451
- 452
- 453



454

455

456

Fig.1 The parallel-plate geometry (Ref: Walters, page 126)

Manuscript-In-Press

Label	MPC		PETA or TEGDMA		DMPA		70% Ethanol
	Conc. (w/v%)	Volume (μ l)	Conc. (v/v%)	Volume (μ l)	Conc. (w/v%)	Volume (μ l)	Volume (μ l)
P1	25	125	3	15	0.5	25	85
P2	25	125	6	30	0.5	25	70
P3	25	125	9	45	0.5	25	55
P4	25	125	12	60	0.5	25	40
P5	25	125	15	75	0.5	25	25
P6	25	125	18	90	0.5	25	10

457
458 Tab.1 Concentrations and volumes of MPC, PETA (or TEGDMA), and DMPA

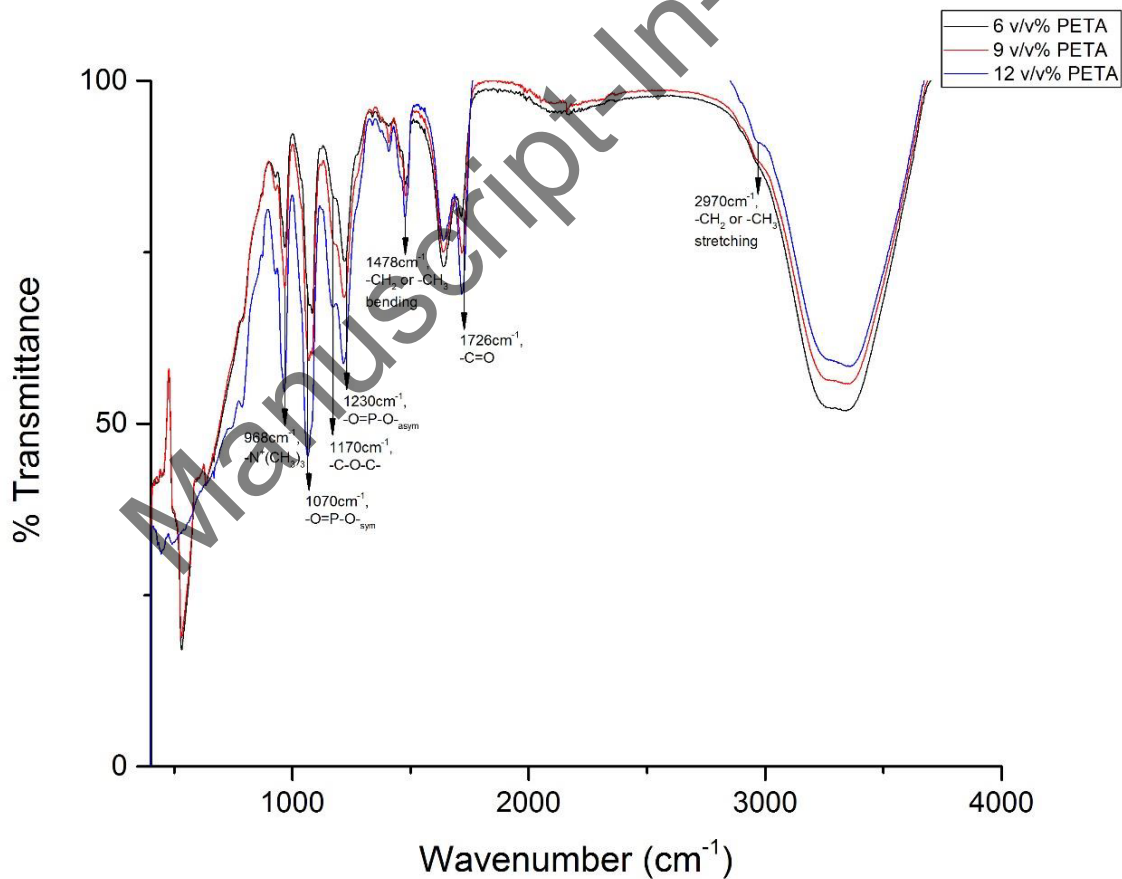


459
460 Fig.2 Specac's Golden Gate™ ATR Accessory (Ref: retrieved from <http://www.specac.com/products/golden-gate-atr-ftir-accessory/standard-golden-gate-diamond-atr-accessory/513>)
461



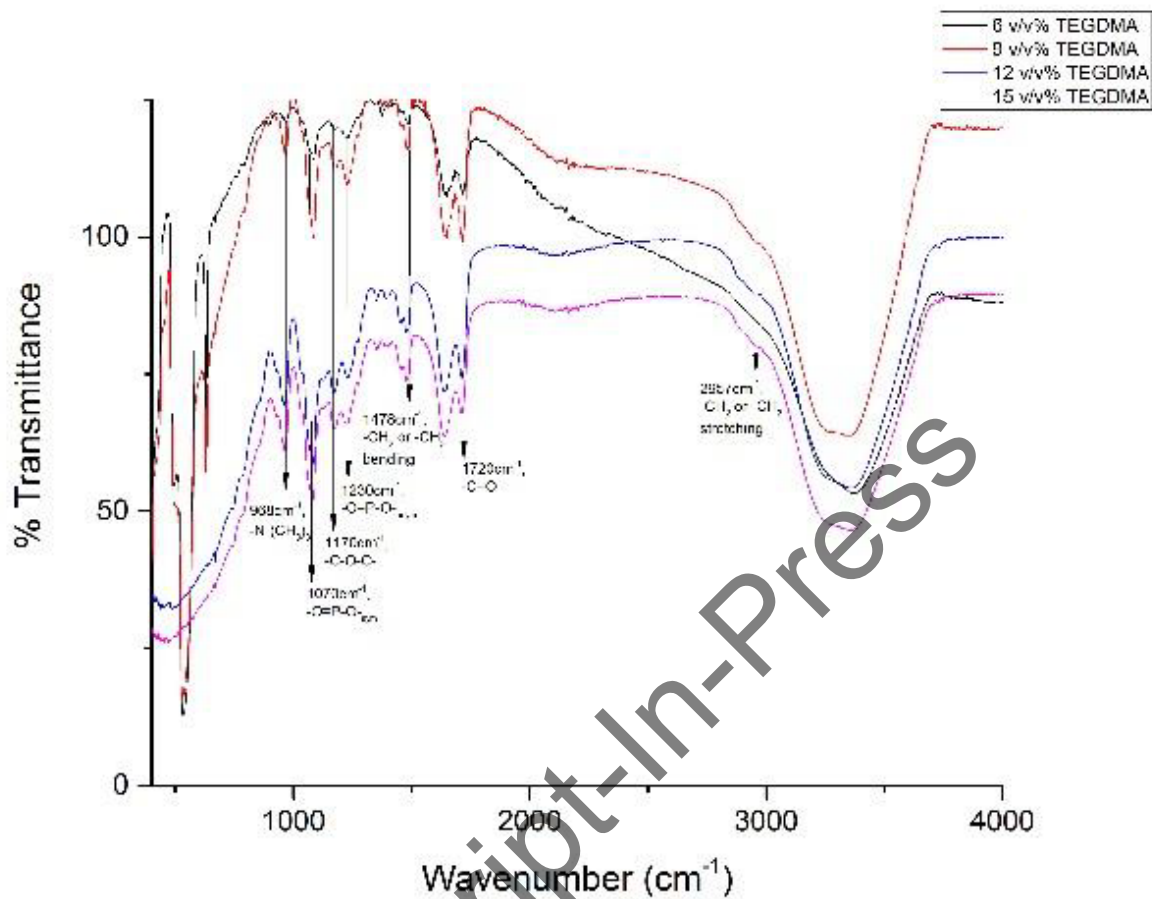
462
463
464

Fig.3 TA instruments rheometer (Ref: retrieved from <http://www.tainstruments.com/dhr-1/>)

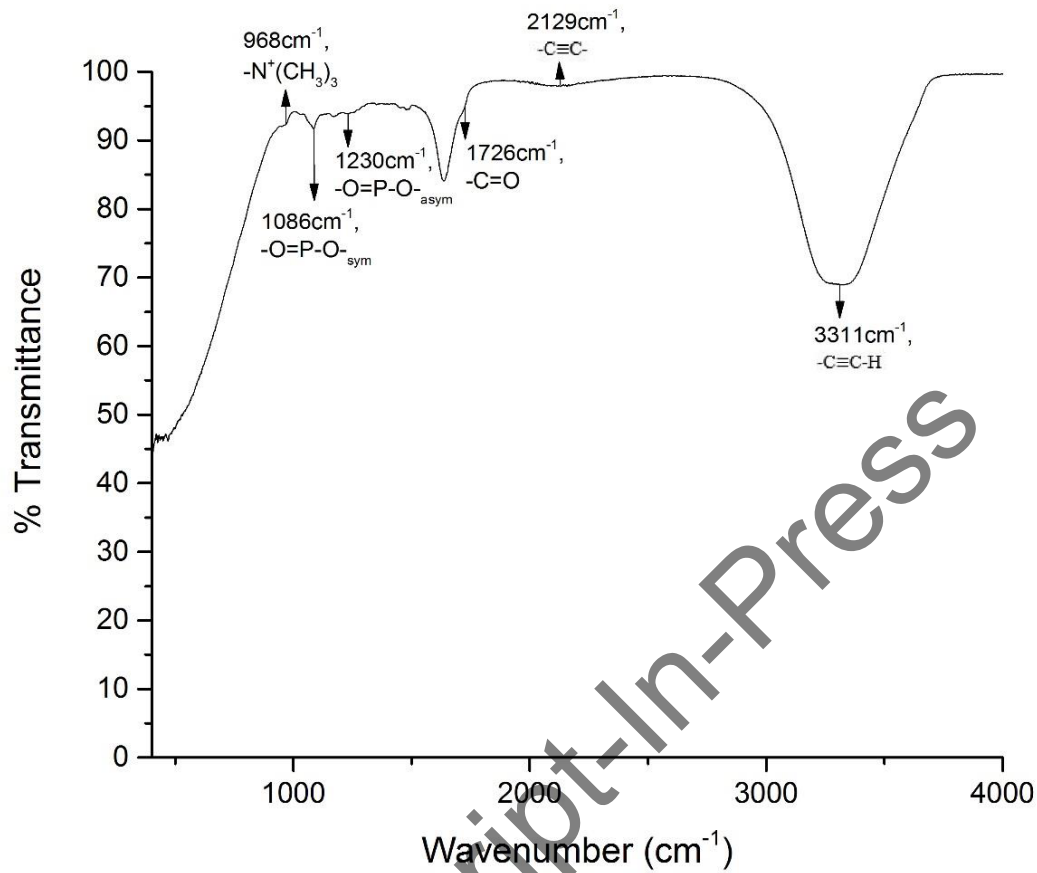


465
466
467

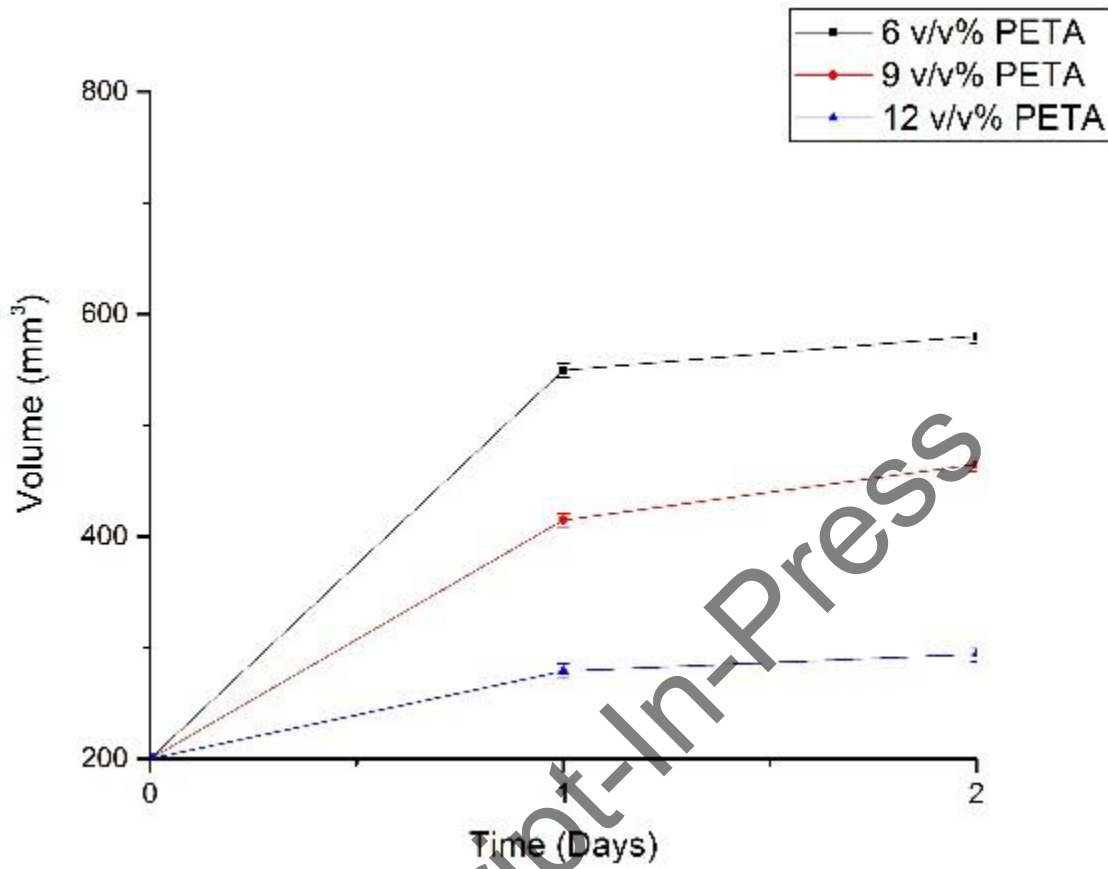
Fig.4 ART-FTIR spectra of poly(MPC) hydrogel crosslinked with PETA. MPC was 25 w/v% in all cases. w/v% of PETA shown on the graph. Characteristic peaks were indicated with wavenumbers and corresponding functional groups.

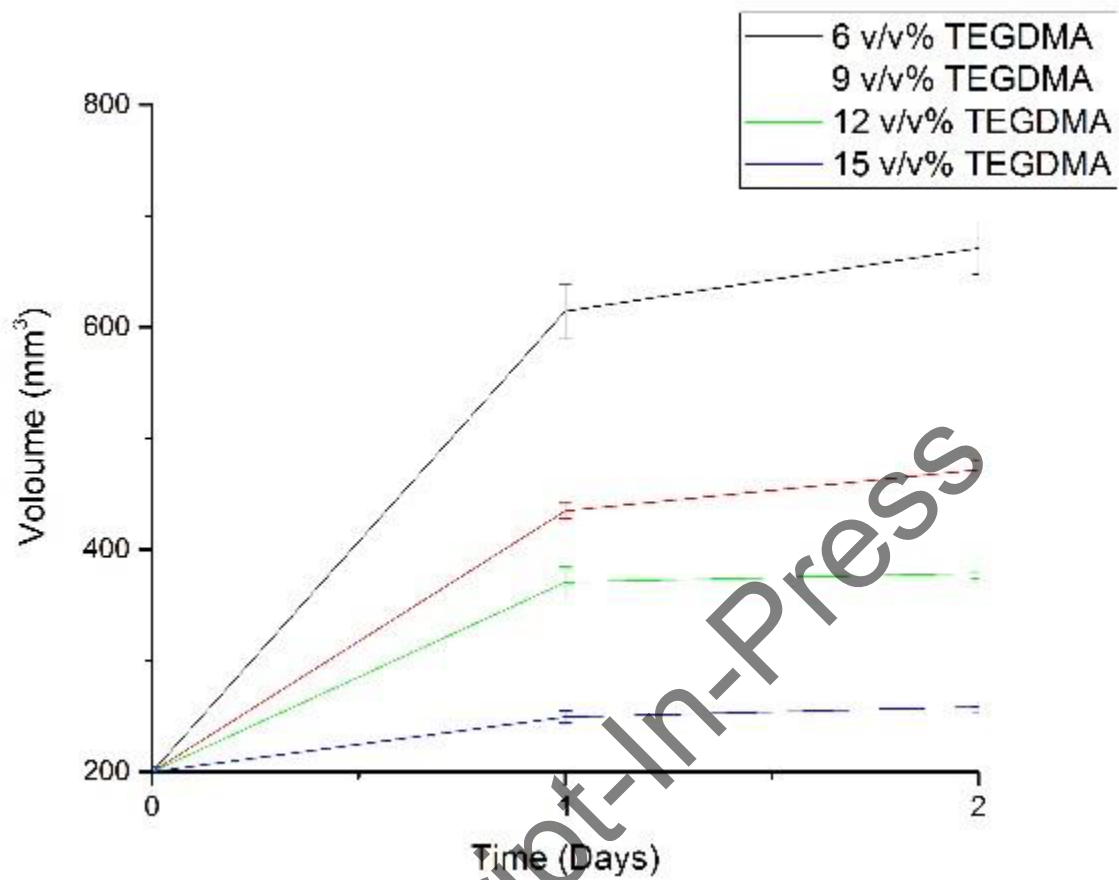


468
 469 Fig.5 ATR-FTIR spectra of poly(MPC) hydrogel crosslinked with TEGDMA. MPC was 25 w/v% in all cases. w/v% of
 470 TEGDMA shown on the graph. Characteristic peaks were indicated with wavenumbers and corresponding functional groups.

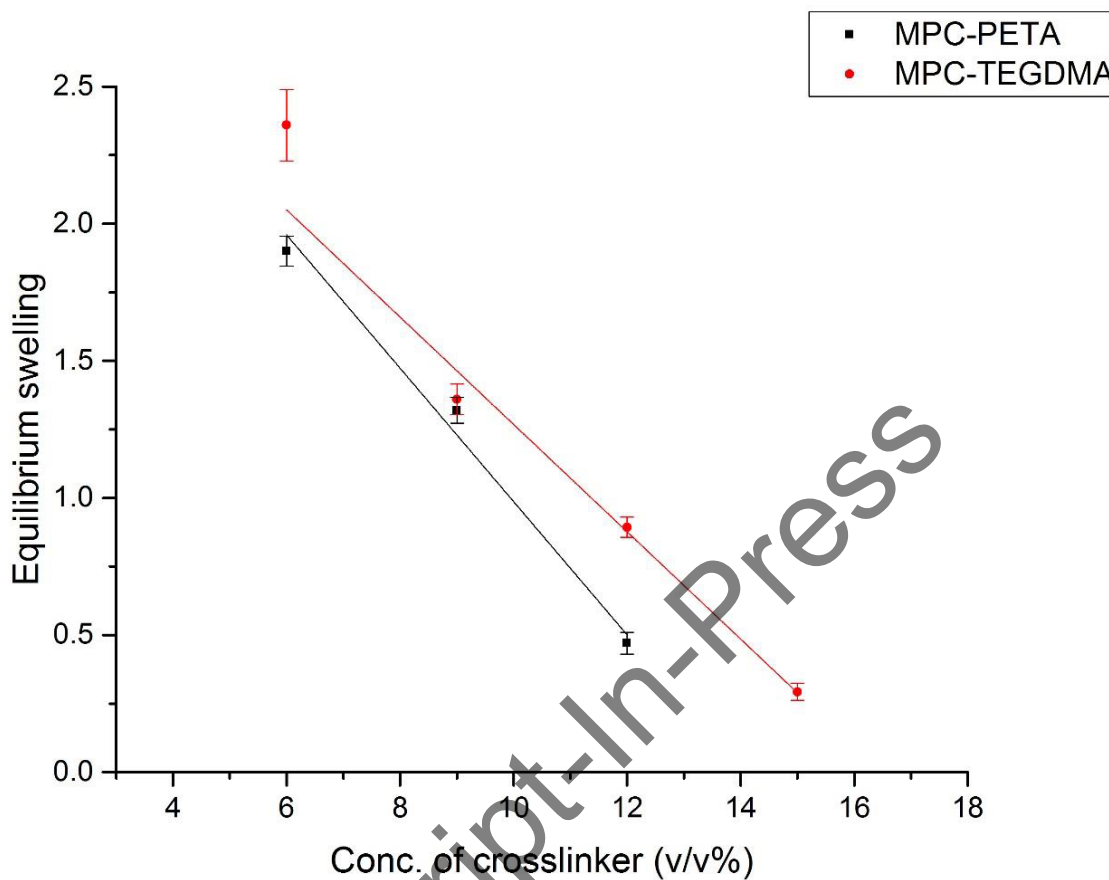


471
472 Fig.6 ATR-FTIR spectrum of poly(MPC) hydrogel (25w/v%) crosslinked with 15 v/v% TEGDMA and 3 v/v% PgMA.
473 Characteristic peaks were indicated with wavenumbers and corresponding functional groups.

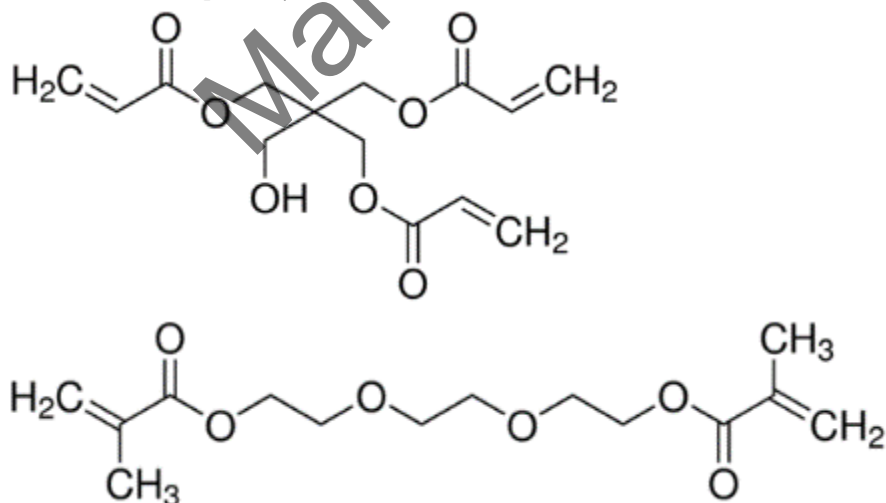




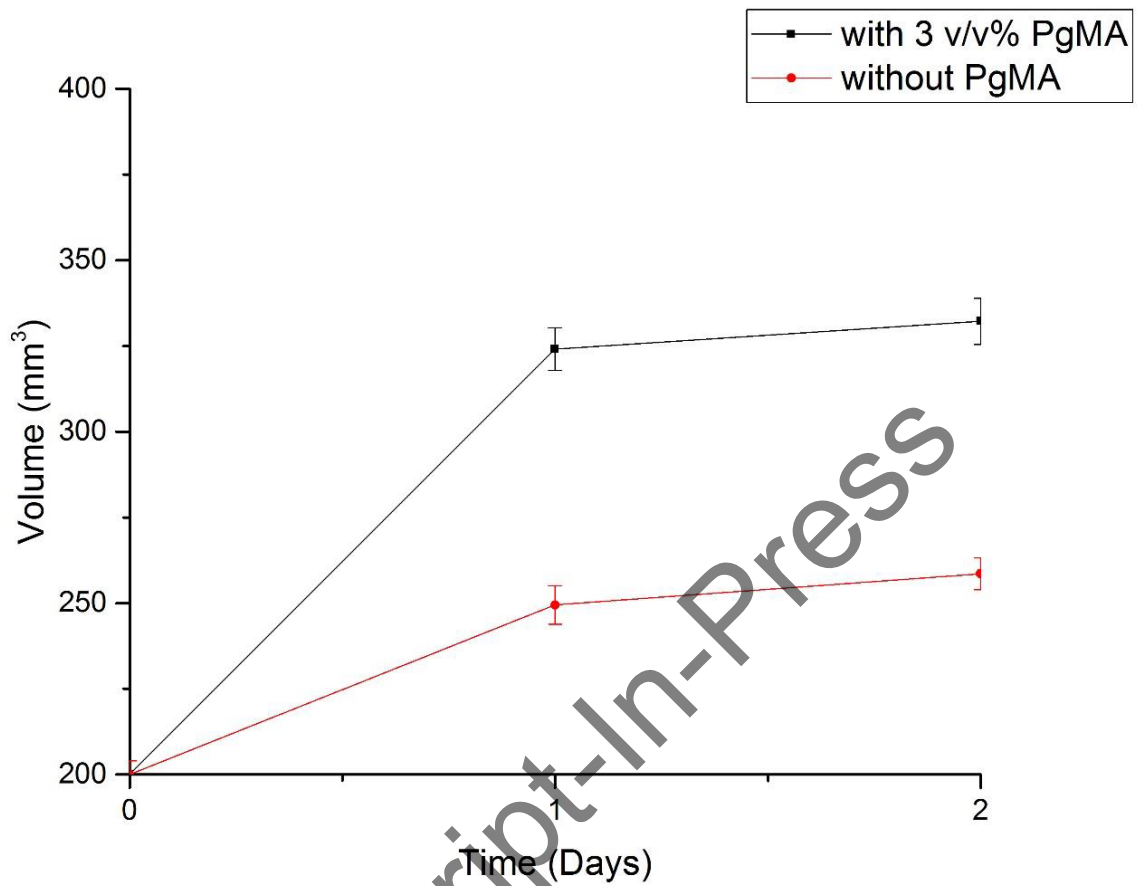
475
 476 Fig. 7 & 8 Volume of poly(MPC) hydrogel crosslinked with PETA (top) and volume of poly(M) hydrogel crosslinked with
 477 TEGDMA (bottom) as function of time. MPC was 25 w/v% in all case. v/v% of PETA and TEGDMA shown on the graph.
 478 Symbols and error bars showed mean and standard deviation of 3 samples. Solid lines were a guide to the eye.



479
 480 Fig.9 Equilibrium swelling of poly(MPC) hydrogel crosslinked with PETA and poly(MPC) hydrogel crosslinked with
 481 TEGDMA as function of concentration of crosslinkers. Symbols and error bars showed mean and standard deviation of 3
 482 samples. Solid lines were linear fitting lines. Gradients of equilibrium swelling for MPC-PETA and MPC-TEGDMA were -
 483 0.243 and -0.196 respectively.

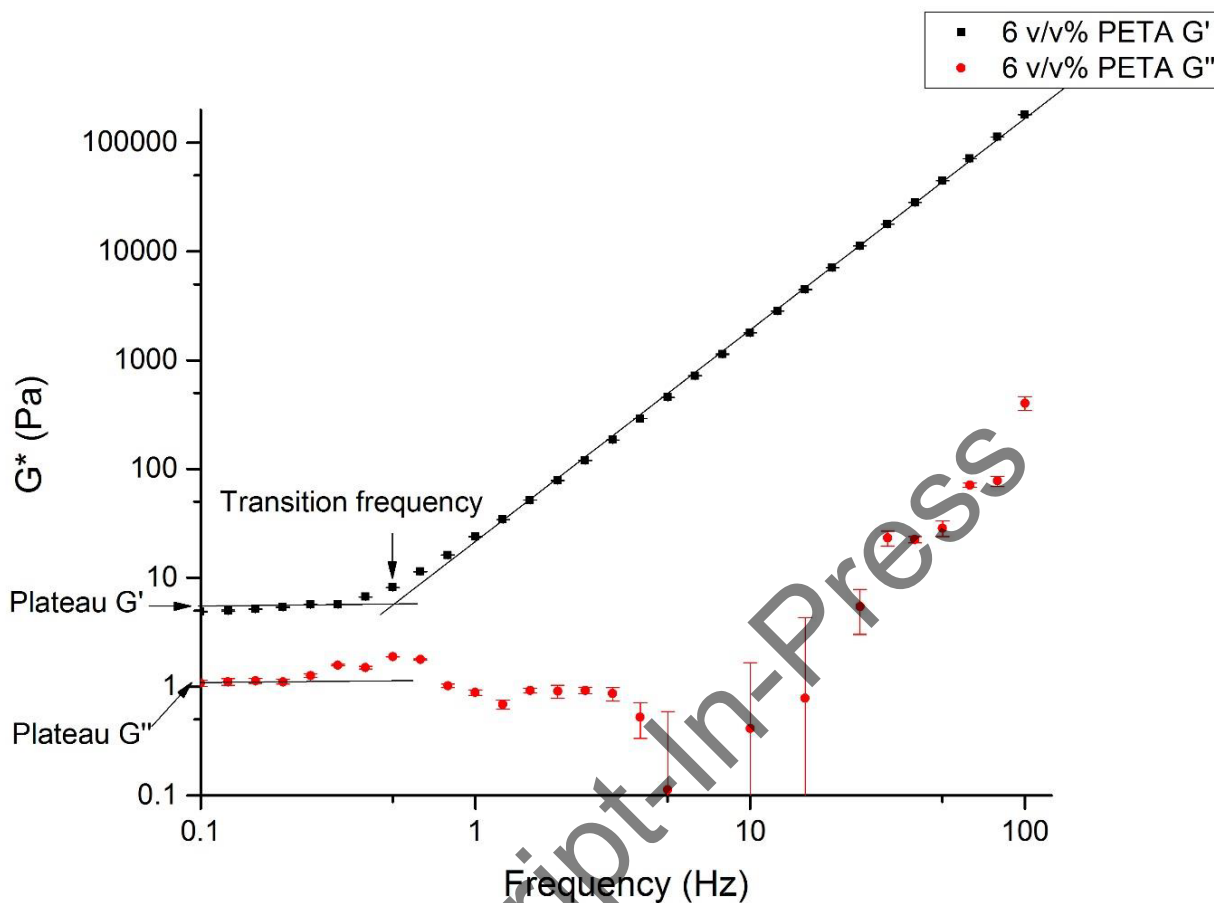


484
 485
 486 Fig.10 & 11 Chemical structures of PETA molecule (left) and TEGDMA molecule (right)

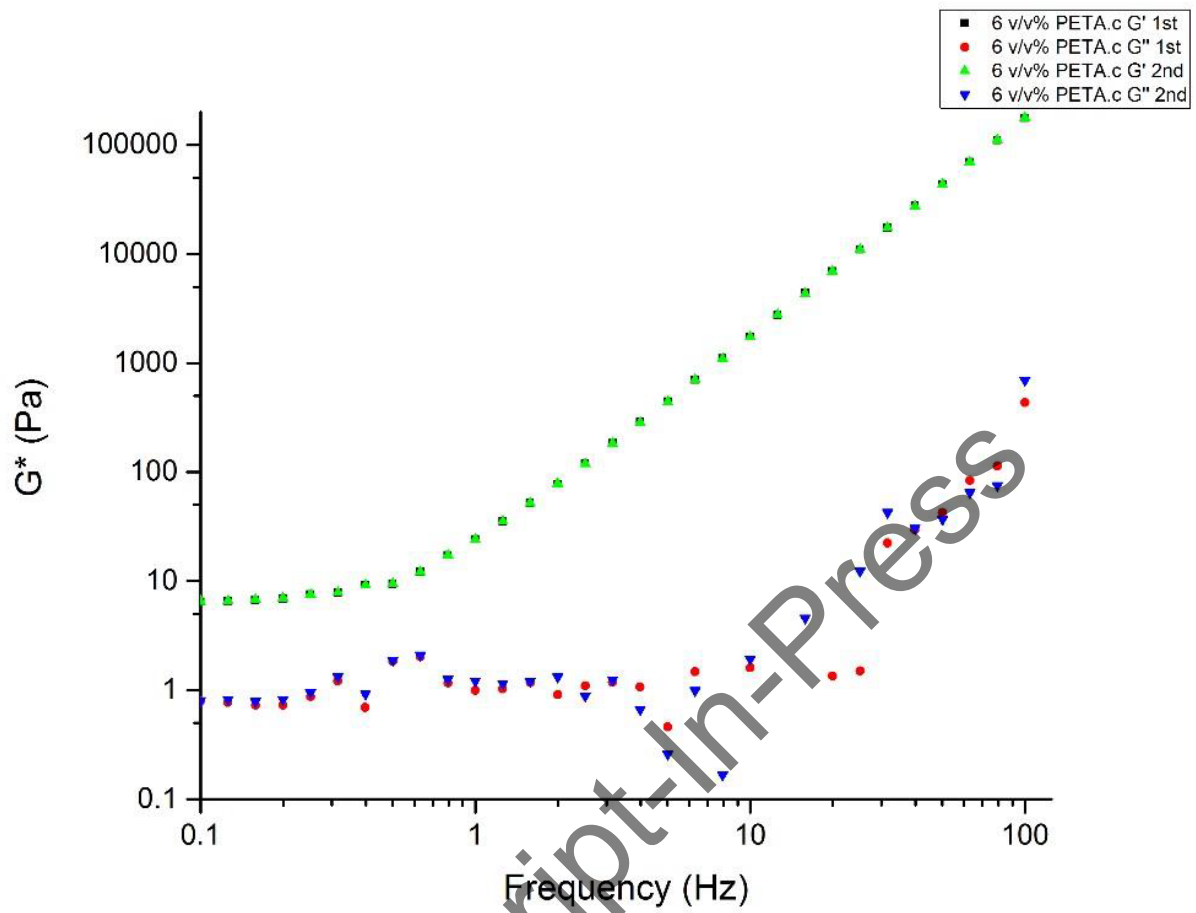


487
488
489
490

Fig.12 Volume of poly(MPC) hydrogel (25w/v%) crosslinked with 15 v/v% TEGDMA, copolymerised with and without 3 v/v% of PgMA. Symbols and error bars showed mean and standard deviation of 3 samples. Solid lines were a guide to the eye.

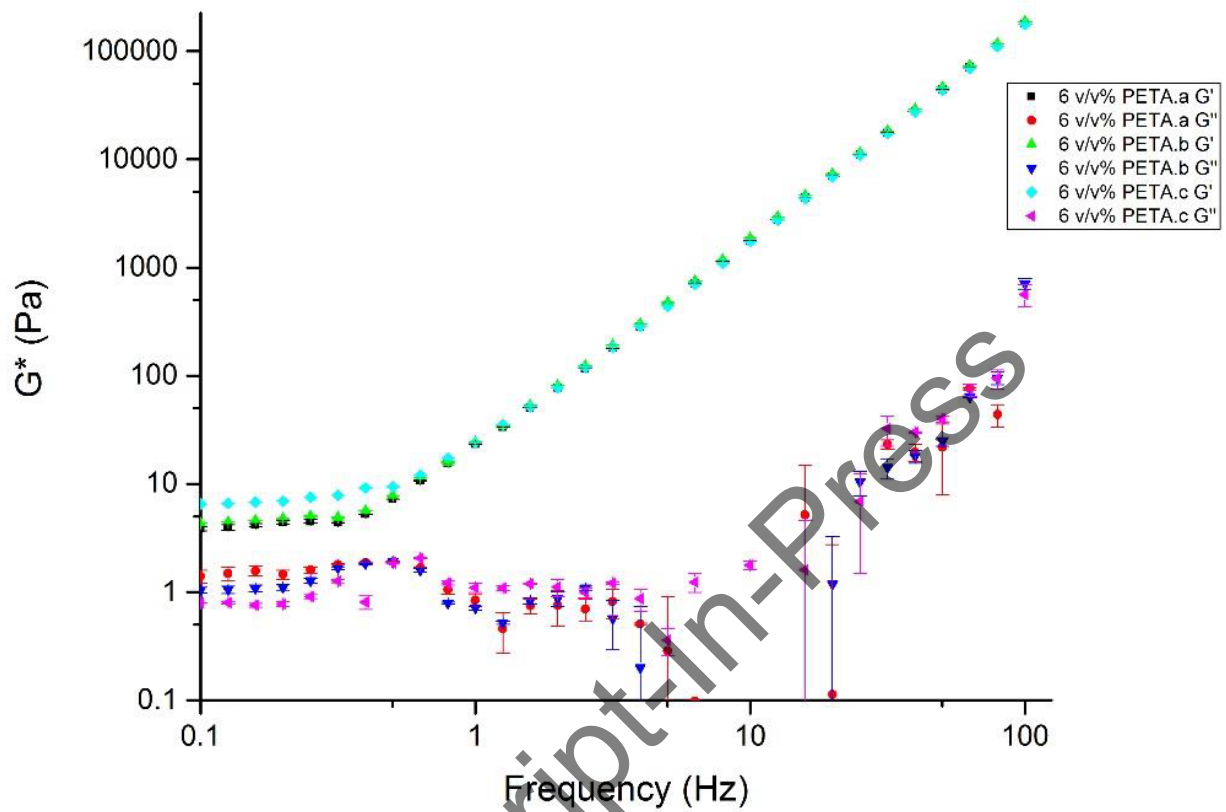


491
 492 Fig.13 Rheology of 25 w/v% poly(MPC) hydrogel crosslinked with 6 v/v% PETA. Symbols and errors bar showed mean and
 493 standard deviation of 3 samples. Solid lines were the gradients of curves and the guide to eyes. The plateau storage moduli
 494 G' and loss moduli G'' were read at the frequency of 0.1Hz. The transition frequency was determined from the interception
 495 of two slopes.



496
497
498

Fig.14 Rheology of 25 w/v% poly(MPC) hydrogel crosslinked with 6 v/v% PETA. One sample (6 v/v% PETA.c) was tested for 2 times under the same conditions for the reliability of experiments.

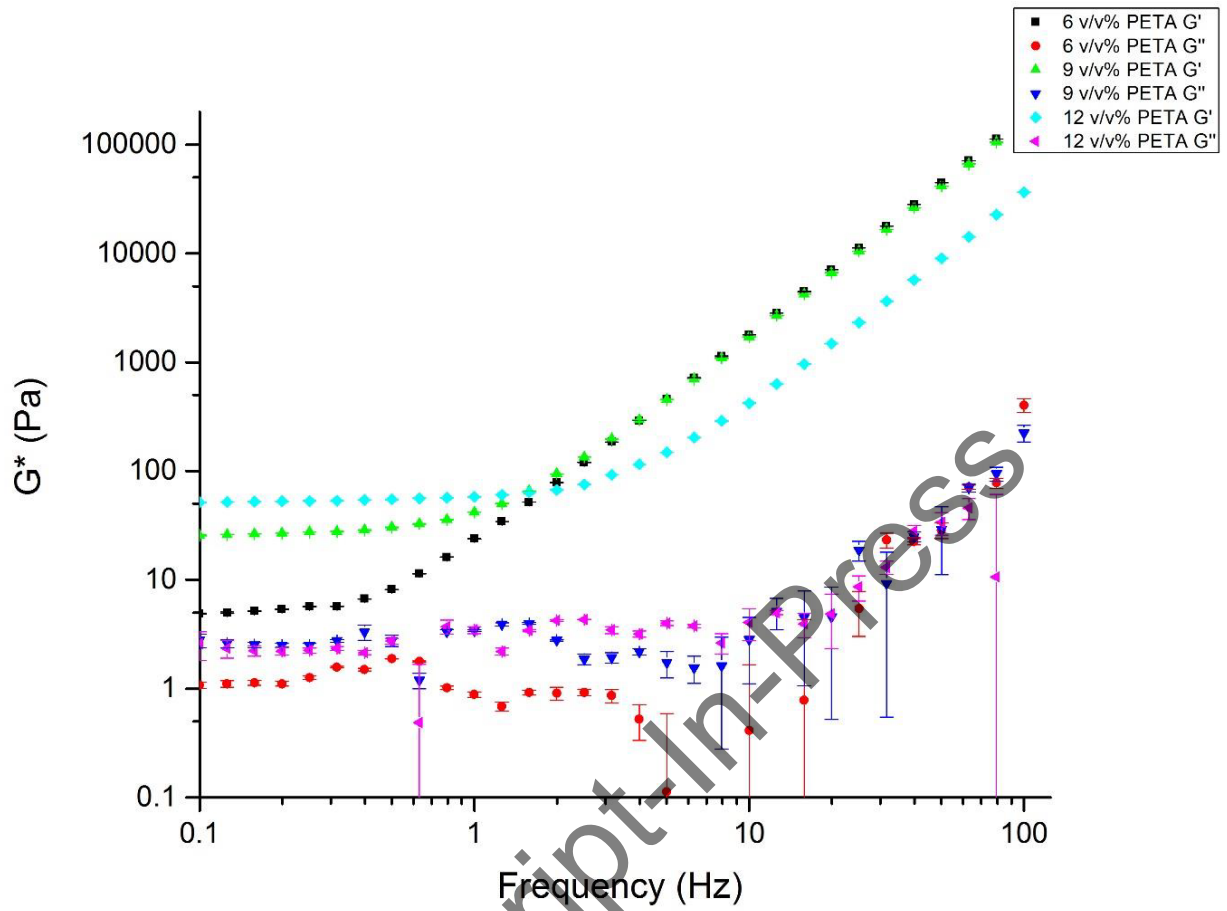


499

500 Fig.15 Rheology of 25% w/v% poly(MPC) hydrogel crosslinked with 6 v/v% PETA. 3 samples (6 v/v% PETA a, b and c) with

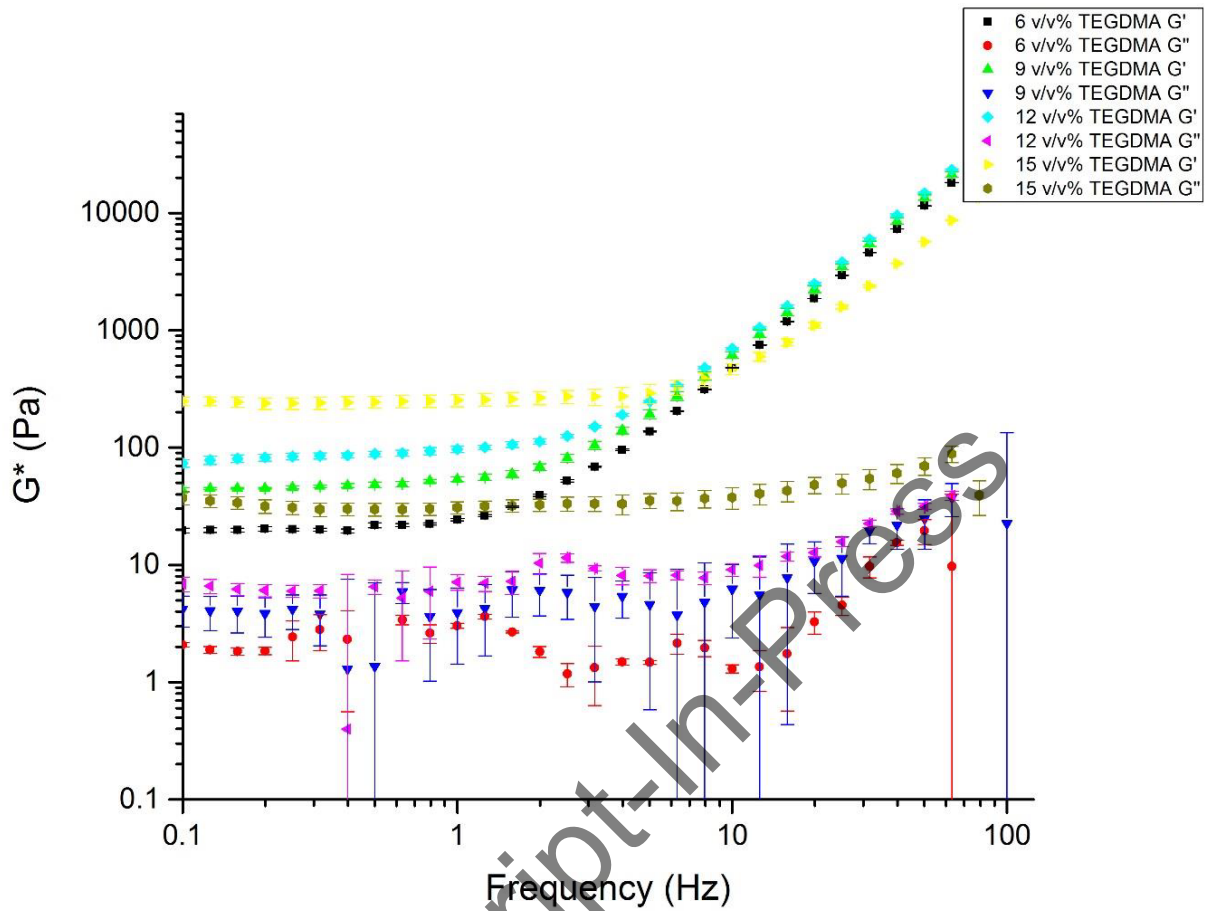
501 the same concentration of PETA were formed and tested for 2 times under the same conditions for the reliability of

502 experiments. Symbols and errors bar show mean and standard deviation of 2 measurements.



503
504
505

Fig.16 Rheology of poly(MPC) hydrogel crosslinked with PETA. MPC was 25 w/v% in all cases. w/v% of PETA was shown on the graph. Symbols and error bars showed mean and standard errors of 3 samples.



506
507
508

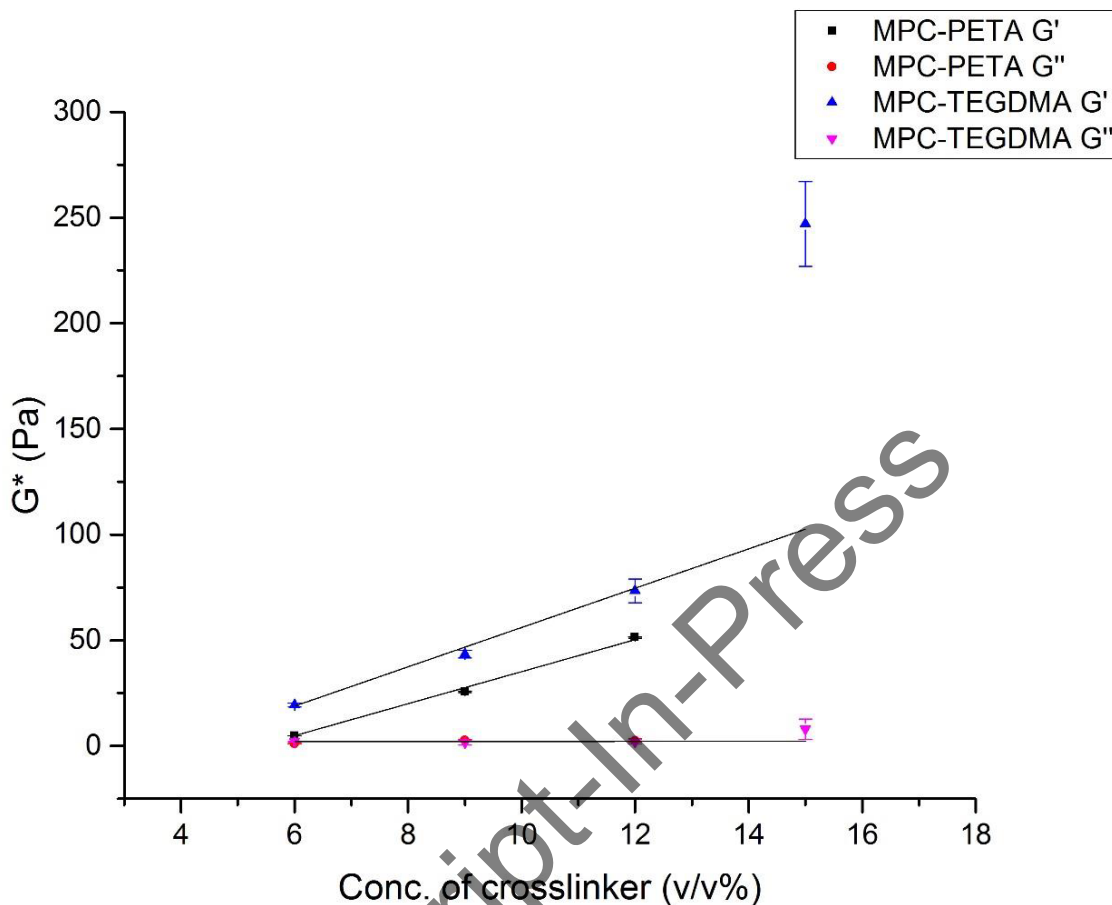
Fig.17 Rheology of poly(MPC) hydrogel crosslinked and TEGDMA. MPC was 25 w/v% in all cases. w/v% of TEGDMA was shown on the graph. Symbols and error bars showed mean and standard errors of 3 samples.

Hydrogel	PETA conc. (v/v%)	Plateau G' (Pa)	Plateau G'' (Pa)	Transition frequency (Hz)	Gradient of G' _{T.F.} - 100Hz
P1	3	-	-	-	-
P2	6	4.88±0.0625	1.08±0.0692	0.501	0.296
P3	9	25.6±0.347	2.78±0.399	1.00	0.310
P4	12	51.4±0.367	2.58±0.761	2.51	0.396
P5	15	-	-	-	-
P6	18	-	-	-	-

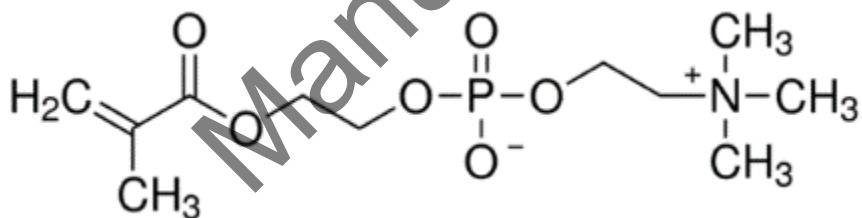
509
 510 Tab.2 &3 Experimental data obtained from rheological measurements of poly(MPC- PETA) hydrogel (top). MPC was 25
 511 w/v% in all case. Plateau G' and G'' at the frequency of 0.1Hz were shown with mean value and standard deviation of 3
 512 samples. Transition frequency was read at the change of gradient of G'.

Hydrogel	TEGDMA conc. (v/v%)	Plateau G' (Pa)	Plateau G'' (Pa)	Transition frequency (Hz)	Gradient of G' _{T.F.} - 100Hz
T1	3	-	-	-	-
T2	6	19.4±0.906	2.08±0.0915	1.26	0.341
T3	9	43.5±1.81	4.18±1.23	1.58	0.372
T4	12	73.4±5.54	6.89±1.01	1.99	0.467
T5	15	247±20.1	7.94±4.75	7.94	0.313
T6	18	-	-	-	-

513
 514 Tab.3 Experimental data obtained from rheological measurements from poly(MPC-TEGDMA) hydrogel.



515
 516 Fig.18 Plateau G' and G'' of poly(MPC) hydrogel crosslinked with PETA and poly(MPC) hydrogel crosslinked with
 517 TEGDMA as function of concentrations of crosslinkers. Symbols and error bars show mean and standard deviation of 3
 518 samples. Solid lines were linear fitting lines. Gradients of plateau G' for MPC-PETA and MPC-TEGDMA were 7.57 and 9.30



519
 520 Fig.19 Chemical structure of MPC molecule

521
 522